

Comparison of CCD Damage due to 10 and 60 MeV Protons

Gordon R. Hopkinson, *Member, IEEE* and Ali Mohammadzadeh

Abstract-- Dark current and charge transfer inefficiency (CTI) data are presented for four CCD device types after 9.5 and 60 MeV proton irradiation. Comparison of the damage at the two energies allows a test of the validity of NIEL scaling. It was found that the ratio of the damage at 9.5 MeV to that at 60 MeV was 35% higher for the CTI than for the average bulk dark current, for the devices tested. Both the CTI and the dark current showed significant annealing at 150°C.

I. INTRODUCTION

CCDs are especially vulnerable to proton-induced displacement damage and the effects have been extensively studied over the past decade [1]-[3]. However, there are a number of issues that continue to be important. These include:

- the nature of the lattice defects involved and the way the defect inventory varies with particle type and energy
- the corresponding variation in device properties (e.g. dark signal and charge transfer inefficiency)
- the nature of the defects responsible for dark current fluctuations (Random Telegraph Signals) and the characteristics of the fluctuations and how they affect calibration strategies for space instruments.

Knowledge of the types of lattice defects created by proton irradiation is particularly important for space science instruments that operate the CCD at low temperatures. This is because the main defects responsible for charge transfer effects near room temperature can be 'frozen out' by keeping them filled with charge (for example, using LED pre-flashing or charge injection from special input gate structures [4]). The faster traps are still active, however, and tend to dominate the radiation effects in the CCD, but, so far, we have little knowledge of the defects involved or how the trap concentrations may vary with proton energy or the materials composition of the silicon wafer.

The starting point for making device damage calculations is to assume that the damage is proportional to the nonionizing energy loss (NIEL) [5]. This is equivalent to assuming that the relative trap concentrations do not change with proton

energy. NIEL scaling has been observed to hold reasonably well for many devices and, in particular, for CCD charge transfer inefficiency (CTI) [6] and mean dark signal [7]. Hence NIEL scaling is a good first step for damage prediction and allows for most of the damage dependence on particle type and energy. However there is still the possibility that NIEL scaling may not apply at a detailed level.

Recent calculations of the nonionizing energy loss in silicon have been presented by Dale et al. [8], Akkerman et al. [9] and Jun et al. [10]. Whilst consistent, considering the uncertainties involved, there are some important differences. In particular the ratio between the NIEL values at 10 and 60 MeV is 3.3 from [9] compared to 2.2 in the Dale et al data. These two energies are important since 10 MeV is often used for ground testing (because of the irradiation facilities available and because of the ease of masking the device into several fluence regions), whilst protons of energy around 60 MeV predominate in the space environment inside spacecraft (the low energy protons having been removed by shielding). Hence it would be useful to know which value is correct – or even if the same ratio holds for both dark current and charge transfer damage (or for different device types).

The present study arose from a radiation evaluation of several CCD types in support of a programme of the European Space Agency (ESA) for Capability Approval of CCD suppliers. Since the programme called for an extensive device study, the opportunity was taken to use the data to consider further the relation between dark current and CTI damage and the nonionizing energy loss. Although the factor 1.5 discrepancy in NIEL, mentioned above, may seem small, the CCD displacement damage is often critical to mission lifetime and it is important that design margins are not overly conservative. It is hoped that the results of the study will also give some insight into mechanisms of defect generation.

To measure damage ratios accurately it was considered important to irradiate with the two proton energies on the same device. Otherwise any variation in device-to-device response or in test or operating conditions might mask any differences. This was a contributing factor in deciding the highest energy which could be used during this investigation. At 60 MeV it is just possible to shield the device so that part is unirradiated (and so can be used as a reference and/or for later irradiation at a lower energy). It will be seen that the production of secondary protons and neutrons (due to interaction of the primary protons with the material of the

Manuscript received July 22, 2003. This work was funded by the European Space Agency.

Gordon Hopkinson is with Sira Electro-Optics Ltd, South Hill, Chislehurst, Kent, BR7 5EH, UK (telephone +44 (0)208 468 1794, e-mail: gordon.hopkinson@siraeo.co.uk).

Ali Mohammadzadeh is with the European Space Agency, ESTEC, Keplerlaan 1, 2200 AG, Noordwijk, The Netherlands (telephone + 31 71 565 5894), e-mail ali.mohammadzadeh@esa.int.

masking shield) gives significant effects – which are expected to be yet more pronounced should a higher energy be used. 9.5 MeV was chosen as the lower energy so that a comparison could be made with the substantial amount of existing test data at that energy. Note that in future programs (when a greater number of device samples may be available) it would be useful to perform additional damage comparisons at both lower and higher energies (e.g. 1.5 and 100 MeV).

At 9.5 MeV most recoil atoms have low energy and the damage is mainly in point defects; whereas at 60 MeV inelastic collisions are more common, recoil energies are higher and there are far more clusters (see [1] and the references therein and [11]). Hence, if there are any significant differences in defect character between point and cluster damage then this should be apparent in the results.

As well as making a comparison of damage at the two energies, this study also provides a database of damage effects [12]. By measuring trap emission times at several temperatures it is possible to gain some insight into device-to-device differences in trap concentration. Results of high temperature annealing will also be discussed. It will be seen that significant annealing of both dark current and CTI occurs above 100°C.

The opportunity was taken to study the random telegraph signal (RTS) behavior in the proton-irradiated CCDs (particularly for some devices which were irradiated to a low fluence of 9.5 MeV protons so that the chance of more than one RTS defect in a pixel is small and the RTS signals are relatively clear) – however this was not the main focus of the study. This work provides an update to previous studies but cannot be claimed to be an in-depth investigation (which is still required if accurate predictions of occurrence probabilities and temperature behavior are to be made).

Cobalt60 irradiations were also performed on devices of each type so as to give information on total ionizing dose effects. The results will be discussed briefly.

II. EXPERIMENTAL

A. Irradiations

The 60 MeV irradiations were carried out at the Paul Scherer Institute (PSI), Switzerland and the 9.5 MeV at Ebis Iotron Ltd, Harwell UK. These irradiations were unbiased (pins shorted) with the CCDs at room temperature. The devices were masked to produce unirradiated regions (at 60 MeV 8 mm steel was used and at 9.5 MeV, 1.5 mm aluminum). The 60 MeV fluence was $5.9 \cdot 10^{10}$ p/cm² and for 9.5 MeV was $1.7 \cdot 10^{10}$ p/cm². In addition, some devices were irradiated at 9.5 MeV to several fluence levels (up to $3.4 \cdot 10^{10}$ p/cm²). The cobalt60 irradiations were done at ESA ESTEC, under both biased (normal clocked operation) and unbiased conditions, at room temperature and at a dose rate ~ 3 krd(Si)/hr. In all cases, dosimetry was performed by the facility staff and is believed to be accurate to better than $\pm 5\%$. All the irradiations were carried out during May-October 2002. Measurements were typically carried out 1 week after

irradiation and checked again after several months storage at room temperature. There was no significant annealing of CCD parameters at room temperature and this annealing will not be discussed further.

B. Devices

The devices tested, all frame transfer CCDs, are summarized below. The pixel numbers are for the image region (there are an equal number in the storage region, which was shielded from light during use). All except the CCD55-20 had a front illuminated architecture:

- CCD55-20: 770 x 576, 22.5 μ m x 22.5 μ m pixels from e2v Technologies, Chelmsford, UK. Advanced inverted mode operation (AIMO).
 - 1 device 9.5 and 60 MeV protons
 - 1 device cobalt60, biased to 18 krd(Si)
- CCD57-10: 512 x 512, 13 μ m x 13 μ m pixels with antiblooming structures from e2v Technologies, operated with 2 of the 3 clock phases inverted.
 - 2 devices 9.5 and 60 MeV protons
 - 1 device 9.5 MeV protons
 - 1 device cobalt60, biased to 18 krd(Si)
 - 1 device co60, biased 18 krd(Si) + 18 krd(Si) unbiased
- TH7890M 512 x 512 17 μ m x 17 μ m pixels from Atmel, France, inverted (MPP) mode
 - 2 devices 9.5 and 60 MeV protons
 - 2 devices 9.5 MeV protons
 - 1 device cobalt60, biased to 13 krd(Si)
 - 1 device cobalt60, unbiased to 18 krd(Si)

The CCD55-20 was not used for CTI measurements as its inverted mode structure did not allow backwards clocking and use of the FPR technique Tests were also made on Atmel TH7863D CCDs (288 x 384, 23 μ m x 23 μ m pixels) but these were not irradiated at two energies and results will not be discussed in detail. (see [12] for further information).

C. Device Testing

Devices were tested using equipment supplied by Sira Electro-optics Ltd. This included camera electronics which allowed computer control of biases and clock sequences and digitization of the signals to 16 bit. Image Pro Plus software was used for image analysis and Agilent Vee Pro for automatic test sequences.

The devices were mounted in a liquid nitrogen cooled dewar with a heater mounted on a copper heatsink behind the device. This allowed control of the CCD temperature to $\pm 0.1^\circ\text{C}$ over the range -120 to 30°C (measured with a calibrated platinum resistor mounted in the heatsink).

Measurements of dark current were made on the average of 16 images to reduce noise. CTI measurements used the first pixel response FPR method [13],[15]. There are limitations to this technique when the CTI is large and care was taken that data was only used for which the proportional charge loss was small (i.e. avoiding data for very low signal levels).

For both dark current and CTI a damage factor can be defined using

$$\text{Device damage} = \text{damage factor} \times \text{DD} \quad (1)$$

Where DD is the displacement damage dose, that is, the product of the NIEL and the particle fluence.

In all cases the digitized CCD signals (in ADC units) were converted to electrons/pixel using the data derived from Cd109 X-ray calibrations (made before and after the irradiations).

III. RESULTS

A. Proton-induced Dark Signal

Fig. 1 shows a horizontal profile (averaged over several hundred columns) across a 9.5/60 MeV irradiated CCD57-10 device. The ionization-induced dark current (determined from the separate cobalt60 irradiation) was small and the factor 2 difference between the average dark current in the two regions (after allowing for the differences in proton fluence) gives a ratio between the damage at 9.5 MeV and that at 60 MeV of 1.74 ± 0.1 . It can also be seen that the 60 MeV region has 'soft' boundaries due to the effect of interactions of the proton beam with the 8 mm steel mask. This limits the device area that can be used for measurements. The damage factor ratios were similar in the other device types. If we assume a 4% change in extrapolating from 9.5 MeV to 10 MeV (based on the data of [8]) then the dark current damage ratios are as given below:

Dark current damage at 10 MeV/damage at 60 MeV	
CCD55-20 (1 device)	1.67 ± 0.3
CCD57-10 (2 devices)	1.67 ± 0.3
TH7890M (2 devices)	1.86 ± 0.3

It was found that the irradiations at 9.5 MeV all gave very similar dark currents for devices of the same type, Fig. 2 gives some examples of dark current histograms. In all cases the average dark charge and the main peak of the histograms scaled with temperature with an activation energy in the range 0.63 to 0.65 eV as expected, but there is significant field enhancement (lowering of activation energy for the larger dark current spikes) as shown in the example of Fig 3.

Since there was significant field enhancement, the damage histograms were not used to derive the damage constant (as in the method of Marshall [16] and Robbins [17]). Instead the average dark current level was used and the following values obtained (the error values were derived from estimates of the measurement and dosimetry errors):

Damage constant for bulk dark current	
electrons/cm ³ /(MeV/g) at 300 K	
CCD55-20	$(3.4 \pm 0.7) 10^5$
CCD57-10	$(1.6 \pm 0.7) 10^5$
TH7890M	$(1.4 \pm 0.7) 10^5$

These values can be compared with the universal damage constant proposed by Srour and Lo [18]. They give a value of $(1.9 \pm 0.6) 10^5$ electrons/cm³/(MeV/g) at 300 K which is in good agreement with the above. Note that, to derive the

damage constants, an estimate of the active volume is needed. The values used were:

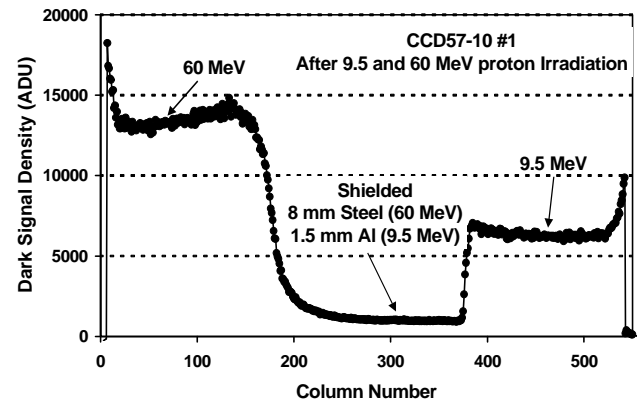


Fig 1 Horizontal profile across a dark image for a CCD57 irradiated with 9.5 and 60 MeV protons

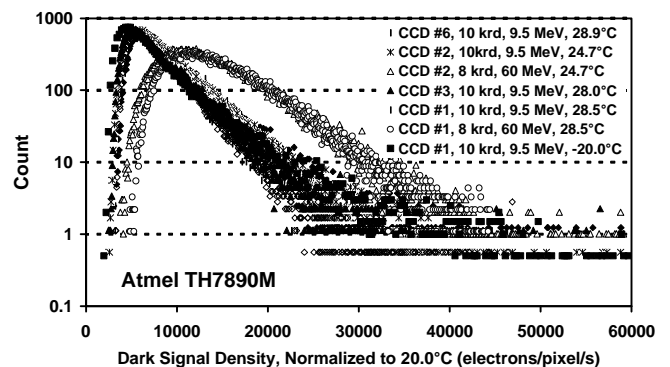


Fig 2 Dark current histograms for Atmel TH7890M devices. The data for device 1 was obtained at both 28.6°C and -20.0°C. The low temperature dark signal density has been scaled assuming an activation energy of 0.63 eV so that it overlays the plot at 28.6°C.

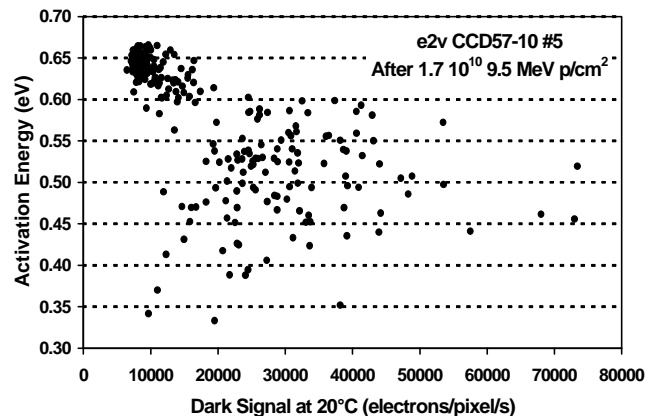


Fig. 3 Activation energy for an e2v CCD57-10 device, measured over the range -400C to 28°C.

	CCD active volume (μm^3)
CCD55-20	1500 (22.5 μm x 16.5 μm x 4 μm)
CCD57-10	500 (13 μm x 9 μm x 4 μm)
TH7890M	750 (17 μm x 11 μm x 4 μm)

One CCD57-10 and one TH7890M device were given an anneal by baking for 3 days at 83°C, then at 110°C and finally at 150°C. The effects in both devices were very similar. Dark current histograms for the TH7890M CCD are shown in Fig. 4. It is seen that there is a significant reduction in the dark

signal nonuniformity, particularly after the final annealing stage at 150°C. Fig 5. Show the estimated annealing factors, which were derived by scaling plots of the horizontal dark current profile (such as Fig 2) so that they could be overlaid. This scaling was found to apply to both the 9.5 and 60 MeV regions, although in the e2v CCD57-10 device the 60 MeV region showed somewhat increased annealing during the final 150°C bake (though since this device was not operated fully inverted, there may be a small contribution due to surface dark current). Also shown in Fig. 5 are results for the charge transfer inefficiency (CTI), which will be discussed later. Annealing of bulk dark current at temperatures in the range 100-150°C has also been observed by Holland [19].

Based on the similarity of the damage constant for a wide variety of devices, Srouf and Lo [18] suggested that device dark current is unlikely to be caused by an impurity related defect but may be due to the divacancy or a multiple vacancy complex. The annealing behavior described above would seem to eliminate the divacancy (since it does not anneal until $\sim 300^\circ\text{C}$ [20]) but a higher order vacancy is not ruled out. Another argument against the divacancy (V_2) is that its level, at ~ 0.43 eV is some way from mid-gap and it is not an efficient generator of dark current. (These arguments have also been put forward by Robbins [17].) In fact, applying standard Shockley Read Hall generation theory [21] with equal hole and electron emission cross sections (σ_p and σ_n), gives a factor 100 difference in generation rate between a midgap state and the divacancy. Mid-gap defects having an energy level ~ 0.55 eV have been found previously but annealing data is either unavailable or ambiguous. Schmidt et al. [22],[23] suggested that their 0.56 eV level is a multivacancy defect but could only confirm that the defect had annealed by 350°C. Ahmed et al. [24] found a defect in proton-irradiated silicon diodes that anneals at around 170°C and tentatively identified it as the four-vacancy (V_4) because of its annealing temperature, though they suggested an energy level of 0.37 eV. Pintille et al [25] also found a level at ~ 0.55 eV but identified it as related to the V_2O complex. However the V_2O defect is known to be stable up to roughly 300°C [20] and so cannot be the main defect responsible for CCD bulk dark current. There is other evidence that there are radiation-induced defects which anneal at around 150°C [26],[27] and these are often associated with the electron paramagnetic resonance (EPR) P3 and P6 centers. These are often identified as the V_4 and di-interstitial (I_2) centers, respectively, but these identifications (and the associated energy levels) are not conclusive (at least in the case of the I_2 [28]). Troxell [29] found a $E_v+0.53$ eV defect in p-type silicon which annealed at $\sim 150^\circ\text{C}$ but the defect was not identified. It should also be noted that many studies have not found mid-gap defects and it can only be concluded that there are many inconsistencies in the literature. Another feature to bear in mind is that many of the proton-induced dark current defects are metastable and give rise to random telegraph signal (RTS) fluctuations [30] as discussed in the next

section. Metastable behavior in intrinsic defects has been suggested (e.g. in the V_2 [31] and I_2 [32]) but, again, the evidence is not conclusive.

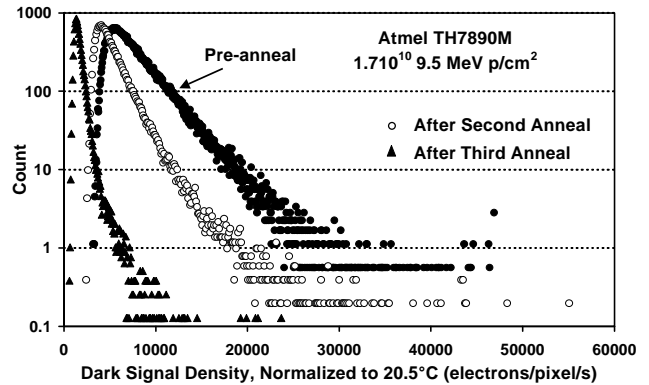


Fig. 4 Dark signal histograms after annealing. The annealing steps were 3 days at 83°C (not shown), followed by 3 days at 110°C and then 150°C.

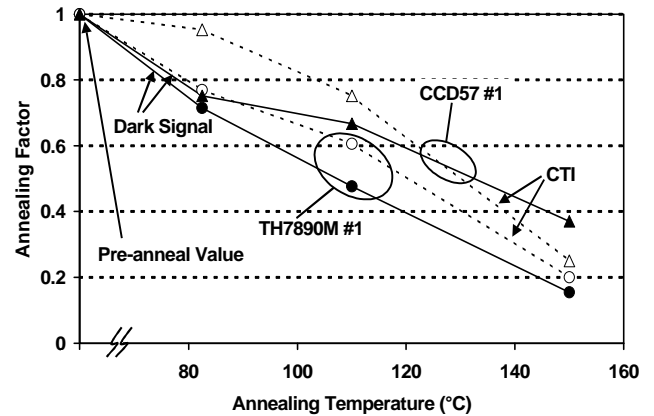


Fig.5 Annealing factors for average bulk dark current, filled symbols (and CTI, open symbols) for the three annealing steps of 83°C, 110°C and 150°C (3 days at each). CCD57: triangles, TH7890M, circles.

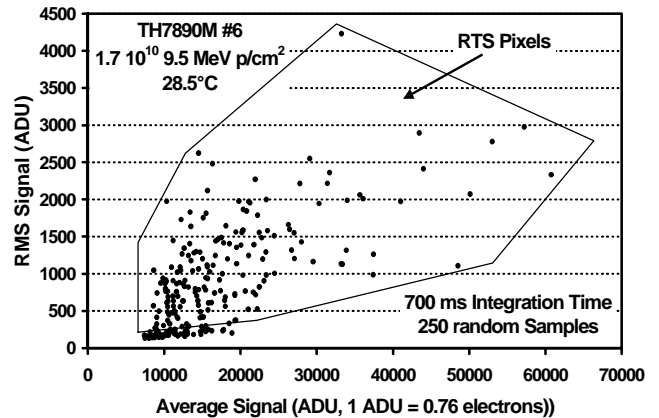


Fig. 6 Identification of RTS pixels for a TH7890M device

B. Measurements of Random Telegraph Signals

For proton irradiated devices some of the defects show metastable behavior so that the dark signal switches between well defined levels, giving the appearance of a random telegraph signal (RTS). This has been studied previously [30] for a limited number of pixels. In this study it was possible to follow sets of several hundred pixels and to analyze the signals at several CCD temperatures. Fig. 6 shows the root

mean square (RMS) signal for a sample of 250 pixels taken at random from the $1.7 \cdot 10^{10}$ p/cm² region of a 9.5 MeV proton irradiated TH7890M. RTS defects can readily be identified as they lie above the shot noise baseline. At this radiation level most pixels show RTS effects. Fig. 7 shows a similar plot for a CCD57-10 device, irradiated to $\sim 5 \cdot 10^8$ 9.5 MeV protons/cm². In this case the dosimetry was rather uncertain and so it was not possible to derive accurate occurrence probabilities, but the number of RTS defects (six in this case) is consistent with the 0.00016 RTS defects/proton/pixel originally found [30]. Other data (so far unpublished) is also consistent with this occurrence probability.

As in previous investigations, some high dark current pixels do not show RTS effects. Fig 8 shows RTS plots at -40°C, so far the lowest temperature at which they have been observed in ground testing - though inflight data [33] suggests that the phenomenon can occur down to much lower temperatures. In this study it was found that the RTS amplitudes varied with temperature with an activation energy of roughly 0.6 eV. The switching time constants were not studied in detail, but the data is consistent with activation energies of 0.9 to 1.6 eV, so that at low temperatures the time constants can be several hours or even days.

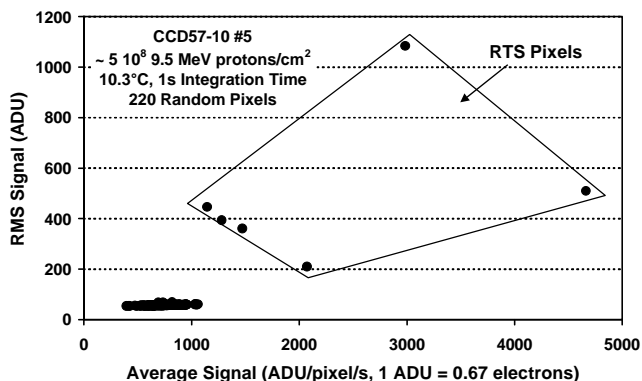


Fig 7. Identification of RTS pixels for a CCD57-10 device

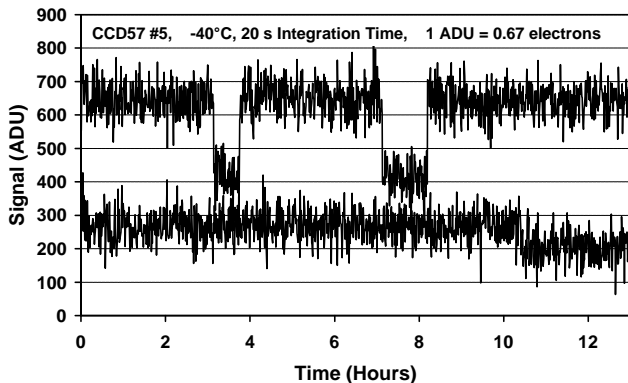


Fig 8. RTS fluctuations at -40°C for a CCD57-10. The CCD integration time was 20s and 1 ADC unit (ADU) corresponded to 0.67 electrons.

The number of RTS pixels decreased after the 3 day anneals at 83°C, 110°C and 150°C (for both the CCD57-10 and TH7890M devices studied). The largest decrease being after the 150°C bake after which nearly all the RTS fluctuations had disappeared (though 2 or three RTS pixels still remained -in samples of 250 random pixels from the 1.7

10^{10} 9.5 MeV p/cm² regions). Hence it is concluded that the RTS pixels show much the same annealing behavior as the average bulk dark current, though the data indicates that annealing was more pronounced for RTS since nearly all the defects were annealed, whereas Fig.5 shows that there is still a significant component remaining for the average dark signal.

C. Measurements of CTI

Fig. 9 shows measurements of trap emission time at several temperatures for both the 9.5 and 60 MeV regions of a typical device. These were made at the same signal level and background. To scale the damage so that the plots coincided, a ratio of 1.47 ± 0.02 was found to apply for all the devices (and in fact for all the CTI measurements at other signal levels, backgrounds and temperatures). That is, the CTI for the 60 MeV region was always greater than that in the 9.5 MeV region by a factor of roughly 1.5. This suggests that the inventory of traps was not significantly different between the 9.5 and 60 MeV regions.

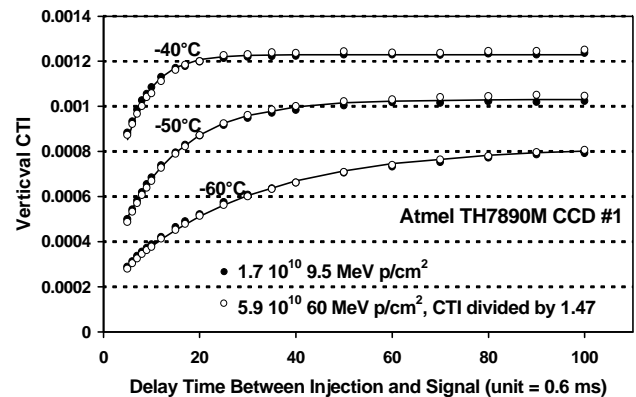


Fig. 9 Trap emission times were found by measuring the CTI as a function of the delay time used in the first pixel response measurement. Dividing the 60 MeV data by 1.47 allowed the plots to be overlapped and this gives an estimate of the ratio between the CTI damage at 9.5 and 60 MeV.

Taking into account the difference in fluence ($5.9 \cdot 10^{10}$ p/cm² at 60 MeV and $1.7 \cdot 10^{10}$ p/cm²) and, as for the average dark signal, a 4% change in extrapolating from 9.51 to 10 MeV, this gives a damage factor ratio (CTI at 10 MeV divided by that at 60 eV) of 2.27 ± 0.1 , very close to the expectation from Dale et al but slightly (and significantly) different from the ratio for dark current. Note that, although dosimetry errors will affect the damage ratio, these errors will be the same for both the dark signal and CTI measurements and so the difference in damage ratio (roughly 1.7 for dark signal and 2.3 for CTI) is significant.

Fig 5. Showed the CTI annealing data. This was obtained by plotting CTI as a function of signal and background and applying scaling factors so that the plots could be overlapped. It was found that a single scaling factor could be used for all signals and backgrounds (that is, the same factor could be used to scale between two annealing steps independent of the particular signal and background conditions used for both the fluence regions). During the annealing the relative

proportions of the traps did not seem to change appreciably; i.e. they seemed to anneal together.

Fig 10 shows the emission time versus temperature for the dominant trapping center both for the present data and that given in Hopkins et al. [34]. Since this indicates a trap energy level of ~ 0.44 eV and the annealing data from Fig. 5 (and from previous studies [19],[35]) show that annealing can occur at 150°C or below, it is presumed that the E center (phosphorous-vacancy) is the main defect involved. The fact that p-channel CCDs show different traps [13],[36] also suggests an impurity related defect.

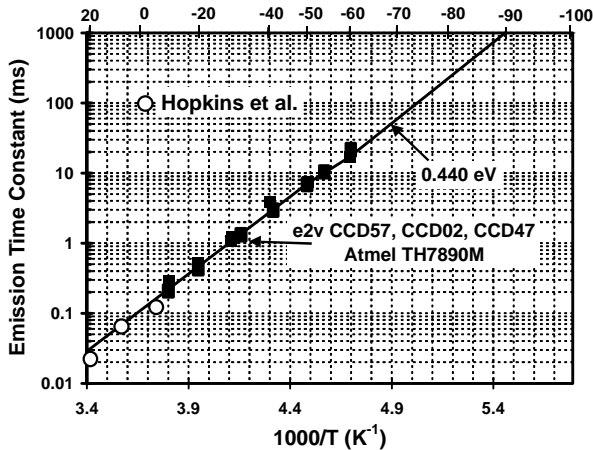


Fig 10. Emission time constant for the dominant trap near room temperature

Although the E center has the highest concentration, there are other traps present [37]. By fitting data such as that shown in Fig. 9 with a multitraps model it is possible to estimate the trap concentration ratios. These show some differences between the CCD types. The fraction of traps that are much faster than the main trap was $\sim 10\%$ for the CCD57-10 but more like 30% for the TH7890M. This may reflect differences in material or manufacturing process. Measurements were also made at temperatures $\sim -100^\circ\text{C}$ where it is possible to distinguish several traps. However, as previously [37], accurate measurements of trap energy levels was not possible, probably because each trap is only dominant for a small temperature range.

Figs 11 and 12 show CTI data for different signals and backgrounds at -30°C for the center of the (frame transferred) image (taking the number of line moves to be the sum of those during frame transfer and readout). The results were very similar for all the devices of a given type and show the expected large variation with signal and background [34],[38]. Measurements were also made for the top and bottom of the image (predominantly fast, $4\mu\text{s}$, line moves and half fast, half slow, $600\mu\text{s}$, line moves, respectively). As expected, the CTI is higher at the bottom of the image and corresponds to a factor ~ 3 difference in the CTI for the two line move speeds.

Data were also obtained at several temperatures. It was again found that simple scaling factors could be applied to each set of data (i.e. each plot of the type shown in figures 11 and 12) to move from one temperature to another. The scaling

factors for the CCD57-10 and TH7890M are shown in Fig. 13. The CCD57-10 CTI reduces by nearly a factor 10 on cooling to low temperatures, as expected since 90% of the traps are E centers and can be kept filled (i.e. inactive). For the Atmel devices, the proportion of E centers was less and so the improvement on cooling was not as high. Interestingly, there is a significant temperature behavior even in the range -20°C to -50°C even though the data in this range always applied to "worst case" CTI where the E centers always have time to emit before a measurement is made.

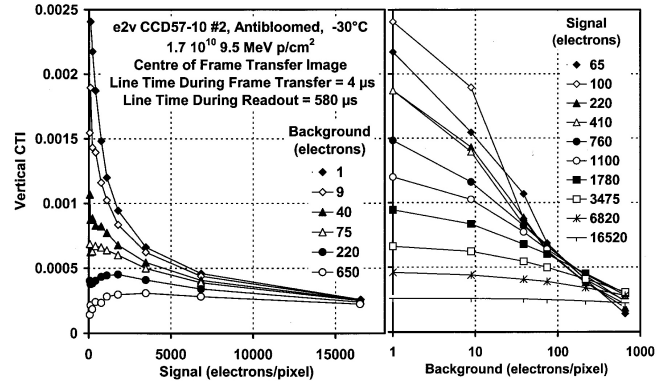


Fig.11 Vertical CTI values as a function of signal and background for a 9.5 MeV irradiated CCD57-10 (centre of frame transfer images)

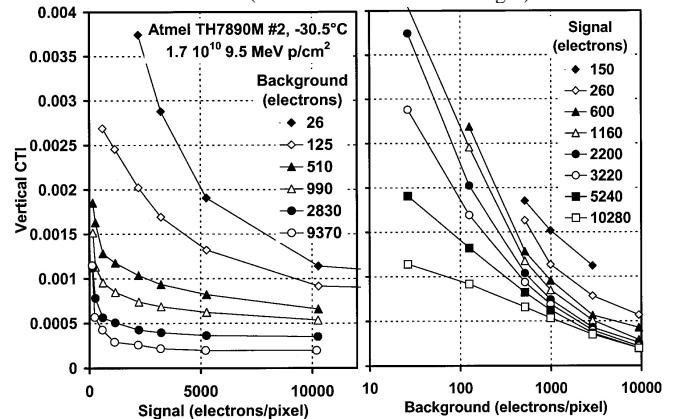


Fig 12 Vertical CTI values as a function of signal and background for a 9.5 MeV irradiated TH7890M (centre of frame transfer images)

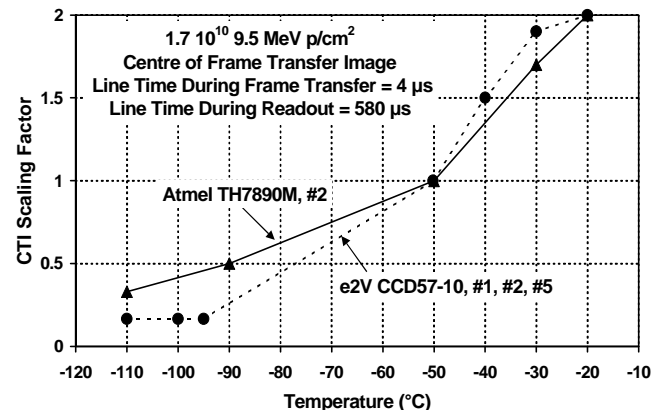


Fig. 13 Vertical CTI as a function of temperature for the CCD57 and TH7890M.

Fig 14 shows the CTI for three types of device, the e2v CCD57-10 and the Atmel TH7890M and TH7863D. Here the CTI values have been scaled so that the plots approximately

overlap. Although there are some differences in shape, particularly at low signals, the overlap is reasonable. The scaling factors (relative to the TH7863 value) reflect the differences in pixel area. That is, at ~ 500 electrons background, the CCD57-10 has a factor 5 lower CTI than the TH7890M and for low backgrounds (30 electrons) the difference is a factor 3. (Note that the CCD57-10 had part of the pixel width taken up with an antiblooming structure so that the volume occupied by the charge, and so the number of traps encountered, is reduced further.)

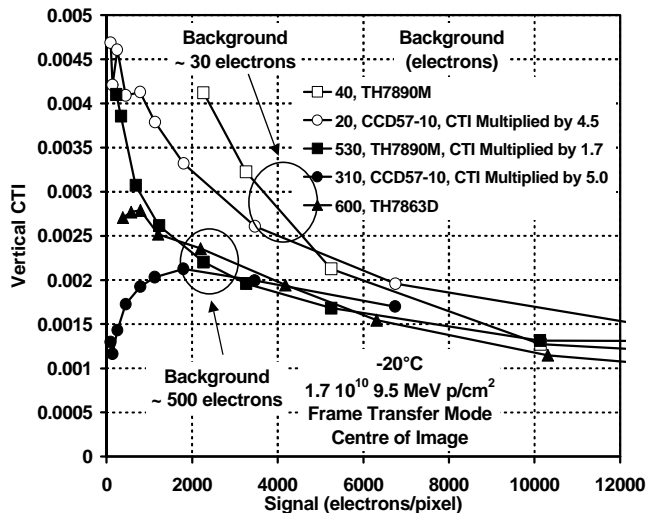


Fig. 14 Comparison of vertical CTI values for the CCD57-10, TH7890M and TH7863D at two background levels. The CTI scaling factors used are shown in the legend.

D. Measurements on Cobalt60 irradiated devices

Ionization damage causes a shift in the flatband voltage and hence an change in the effective voltages applied to the CCD. An important parameter for CCDs is the channel potential at zero gate bias. This is around 10 or 11 V for e2v and Atmel devices but increases with total ionizing dose. The most important consideration is that charge can be transferred to, and read out from, the output amplifier. For pre-radiation testing the CCDs were operated with the manufacturer's datasheet voltages. It was found that the Atmel CCDs did not require voltage adjustments in order to remain operational as there was enough voltage margin to accommodate the flatband voltage shift. With the e2v CCDs it was necessary to reduce the clock low voltages by 1 to 2.5 V (depending on the dose) in order to maintain readout through the output amplifier. In addition, the electronics system used to operate the CCDs had a fixed maximum of 30 V for the drain supply to the CCD amplifier and this resulted in a reduced gain for the e2v devices after irradiation, but this was allowed for in the calibration (the effect being of the order of 20%).

Once the operating voltages had been optimized after irradiation the only other effect of a flatband voltage shift was to change the voltage at which the surface becomes inverted. At this point the surface dark current is greatly reduced, particularly in the CCD55 and TH7890M which are inverted mode operation (or multi phase pinned, MPP) CCDs, where

an implant ensures that the surface under all clock phases can be fully inverted. The shift in inversion voltage was used to accurately measure the flatband voltage shift (see fig. 15). The values obtained were in the range 0.14 to 0.15 V/krd(Si) for biased devices and 0.02 to 0.03 V/krd(Si) for unbiased devices and no annealing was observed even after several months storage at room temperature. These findings are consistent with previous results, though the shift for biased devices seems to have increased slightly (0.1 V/krd(Si) was found previously).

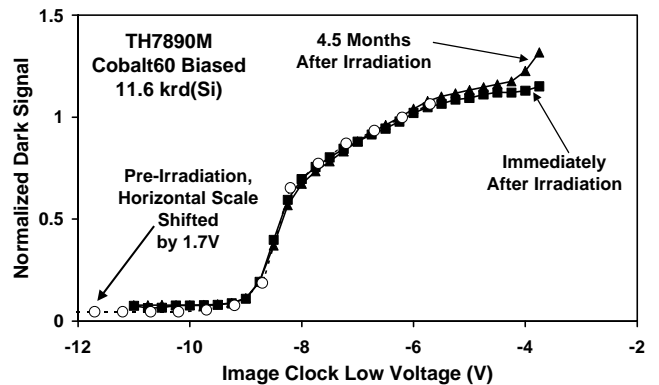


Fig 15. Normalized dark signal versus image clock low voltage, showing the reduction which occurs when the CCD surface becomes inverted. The voltage values for the pre-irradiation data have been shifted (decreased) by 1.7 V.

Since the CCD55 and the TH7890M devices were inverted mode operation, the surface dark current was almost completely suppressed and the dark current due to total ionizing dose was negligible. Except that the CCD55 showed a slightly increased dark signal for regions corresponding to metallizations on the back surface (forming the store shield and dark reference regions - recall that this was a back illuminated device). It is thought that hydrogen (or some similar chemical species) is released from the metallized regions on the back surface and diffuses to the front surface (and the dielectric layer) and enhances the rate of interface trap formation. There was also a component at the extreme edges of the device which appears to be associated with the region outside the active area.

The CCD57-10 could only be operated with two of the three clock phases inverted. Nevertheless the cobalt60-induced dark current was small, being ~ 0.03 nA/cm²/krd(Si) at 20°C for the biased device. As with the CCD55 there was an additional dark current component at the extreme edges of the device (see the start and end of the profile in fig. 1).

No significant changes in full well capacity, responsivity or response nonuniformity were seen, up to the maximum total dose of 18krd(Si).

IV. DISCUSSION

The ratio of the CTI damage at 10 and 60 MeV ($=2.27$) agrees well with the NIEL curves given in [6], [9] and [11] but the dark current ratio is $\sim 35\%$ higher, indicating that the defects responsible are slightly more prevalent in damage from high energy recoils. Although Dale et al [9] have

suggested that departures from recoil equilibrium can arise for high energy protons, we find no evidence for this in the particular results discussed here (comparing the back illuminated CCD55 with the front illuminated CCD57 and TH7890M). Since the CCD57 devices show a small dark current component due to ionization damage, we cannot be sure that this has been completely allowed for but, since the ionization damage varies more strongly with energy than NIEL (by a factor 4 between 10 and 60 MeV), any component due to ionization will increase the discrepancy between the dark current and CTI displacement damage ratios.

The data is consistent with the E center being the primary defect involved in CTI damage, but the defect responsible for bulk dark current is unknown (though the evidence suggests that it is not impurity related and that it anneals at temperatures in the range 100-150°C).

V. ACKNOWLEDGMENT

Wojtek Hajdas (PSI), Keith Jones (Ebis Iotron Ltd) and Bob Nickson (ESA) are thanked for their help in performing the irradiations.

VI. REFERENCES

- [1] C. J. Marshall and P. W. Marshall, "Proton effects and test issues for satellite designers, part B: displacement damage effects", 1999 IEEE NSREC Short Course Notes, pp. IV-50-IV-110.
- [2] G. R. Hopkinson, C. J. Dale, and P. W. Marshall, "Proton effects in CCDs", IEEE Trans. Nucl. Sci., vol. 43, no. 2, pp. 614-627, Apr 1996.
- [3] J. C. Pickel, A. H. Kalma, G. R. Hopkinson, and C. J. Marshall, "Radiation effects on photonic imagers – a historical perspective", IEEE Trans. Nucl. Sci., vol. 50, no. 3, pp. 671-688, Jun 2003.
- [4] M. Giavalisco, "Minimizing CTE losses in the WFC3 CCDs: post flash vs. charge injection", Instrument Science Report WFC3 2003-01, Space Telescope Science Institute. Available on-line at <http://www.stsci.edu/instruments/wfc3/ISRs/WFC3-2003-01.pdf>.
- [5] G. P. Summers, E. A. Burke, P. Shapiro, S. C. Messenger and R. J. Walters, "Damage correlations in semiconductors exposed to gamma, electron and proton radiations", IEEE Trans. Nucl. Sci., vol. 40, no. 6, pp. 1372-1379, Dec. 1993.
- [6] C. Dale, P. Marshall, B. Cummings, L. Shamey and A. Holland, "Displacement damage effects in mixed particle environments for shielded spacecraft CCDs", IEEE Trans. Nucl. Sci., vol. 40, no. 6, pp. 1628-1637, Dec. 1993.
- [7] R. Germanicus, et al. "Evaluation and prediction of the degradation of a COTS CCD induced by displacement damage", IEEE Trans. Nucl. Sci., vol. 49, no. 6, pp. 2830-2835, Dec. 2002.
- [8] C. J. Dale, L. Chen, P. J. McNulty, P. W. Marshall and E. A. Burke, "A comparison of Monte Carlo and analytical treatments of displacement damage in Si microvolumes", IEEE Trans. Nucl. Sci., vol. 41, no. 6, pp. 1974-1983, Dec. 1994.
- [9] A. Akkerman, et al. "Updated NIEL calculations for estimating the damage induced by particles and g rays in Si and GaAs", Radiation Physics and Chemistry, vol. 62, pp. 301-310, 2001.
- [10] I. Jun et al., "Proton nonionizing energy loss (NIEL) for device applications", presented at the IEEE Nuclear and Space Radiation Effects Conference, Monterey, CA, July 2003.
- [11] M. Huhtinen, "Simulation of non-ionising energy loss and defect formation in silicon", Nucl. Inst. Meth. A, vol. 491, pp. 194-215, 2002.
- [12] G. R. Hopkinson, "Radiation testing of CCD and APS imaging devices", European Space Agency Contract Report, available on-line at https://escies.org/public/radiation/esa/database/239DO53FinalReport_iss2.pdf
- [13] G. R. Hopkinson, "Proton damage effects on p-channel CCDs", IEEE Trans. Nucl. Sci., vol. 46, no. 6, pp. 1790-1796, Dec. 1999.
- [14] A. Waczynski et al. "A comparison of charge transfer efficiency measurement techniques on proton damaged CCDs for the Hubble Space Telescope Wide-Field Camera 3", IEEE Trans. Nucl. Sci., vol. 48, no. 6, pp. 1807-1814, Dec. 2001.
- [15] J. R. Janesick, "Scientific Charge-Coupled Devices", Ch. 5, (SPIE Press, Bellingham, 2001).
- [16] P. W. Marshall, C. J. Dale and E. A. Burke, "Proton-Induced Displacement Damage Distributions in Silicon Microvolumes", IEEE Trans Nucl. Sci., vol. 37, no. 6, pp. 1776-1783, Dec. 1990.
- [17] M. S. Robbins, "High-energy proton-induced dark signal in silicon charge coupled devices", IEEE Trans Nucl. Sci., vol. 47, no. 6, pp. 2473-2479, Dec. 2000.
- [18] J. R. Srour and D. H. Lo, "Universal damage factor for radiation-induced dark current in silicon devices", IEEE Trans. Nucl. Sci., vol. 47, no. 6, pp. 2451-2459, Dec. 2000.
- [19] A. D. Holland, "Annealing of proton-induced displacement damage in CCDs for space use", Proc 10th Symposium on Photoelectronic Image Devices, Inst. Phys. Conf. Ser. No. 121, pp. 33-40, 1992.
- [20] J. W. Corbett et al., "The status of defect studies in silicon", Inst. Phys. Conf. Ser. No. 31, pp. 1-11, 1977.
- [21] S. M. Sze, Physics of Semiconductor Devices, 2nd Ed., Wiley-Interscience, New York, 1981, p 90.
- [22] D. C. Schmidt, J. F. Barbot, C. Blanchard and E. Ntsoenzok, "Defect levels of proton-irradiated silicon with a dose of $3.6 \times 10^{13} \text{ cm}^{-2}$ ", Nucl. Inst. Meth. B, vol. 132, pp. 439-446, 1997.
- [23] D. C. Schmidt et al., "Studies of deep levels in He⁺-irradiated silicon", Appl. Phys. A, vol. 65, pp. 403-406, 1997.
- [24] M. Ahmed, S. J. Watts, J. Matheson and A. Holmes-Seidle, "Deep-level transient spectroscopy studies of silicon detectors after 24 GeV proton irradiation and 1 MeV neutron irradiation", Nucl. Inst. Meth. A, vol. 457, pp. 588-594, 2001.
- [25] I. Pintille, E. Fretwurst, G. Lindstroem and J. Stahl, "Close to midgap trapping level in ⁶⁰Co gamma irradiated silicon detectors", Appl. Phys. Lett., vol. 81, no. 1, pp. 165-167, July 2002.
- [26] L. Sealy, R. C. Barklie, W. L. Brown and D. C. Jacobson, "Annealing of defects created in silicon by MeV ion implantation", Nucl. Inst. Meth. B, vol. 80/81, pp. 528-531, 1993.
- [27] H. Lutgemeier and K. Schnitzke, "Paramagnetic centres in proton-irradiated silicon", Phys. Lett., vol. 25A, no. 3, pp. 232-233, 1967.
- [28] B. J. F. Coomer, "A first principles study of radiation defects in semiconductors", Ph.D. Thesis, Univ. of Exeter, UK, Nov. 2000.
- [29] J. R. Troxell, "Ion-implantation associated defect production in silicon", Solid State Electron., vol. 26, no. 6, pp. 539-548, 1983.
- [30] I. H. Hopkins and G. R. Hopkinson, "Further measurements of random telegraph signals in proton irradiated CCDs", IEEE Trans. Nucl. Sci., vol. 42, no. 6, pp. 2074-2081, Dec. 1995.
- [31] E. G. Sieverts and J. W. Corbett, "The neutral divacancy in silicon", Solid State Comm., vol. 43, no. 1, pp. 41-46, 1982.
- [32] J. Kim et al., "Thermally activated reorientation of di-interstitial defects in silicon", Phys. Rev. Lett., vol. 83, pp. 1990-1993, 1999.
- [33] K. P. Klaasen et al. "Inflight performance characteristics, calibration, and utilization of the Galileo SSI camera", Opt. Eng., vol. 36, pp. 3001-3027, 1997.
- [34] I. H. Hopkins, G. R. Hopkinson and B. Johlander, "Proton-Induced Charge Transfer Degradation in CCDs for Near-Room Temperature Applications", IEEE Trans. Nucl. Sci., vol. 41, no. 6, pp. 1984-1990, Dec. 1994.
- [35] J. E. Brau and N. Sinev, "Operation of a CCD particle detector in the presence of bulk neutron damage", IEEE Trans. Nucl. Sci., vol. 47, no. 6, pp. 1898-1901, Dec. 2000.
- [36] C. Bebek et al., "Proton radiation damage in P-channel CCDs fabricated on high-resistivity silicon", IEEE Trans. Nucl. Sci., vol. 49, no. 3, pp. 1221-1225, June 2002.
- [37] G. R. Hopkinson, "Proton-induced charge transfer degradation at low operating temperatures", IEEE Trans. Nucl. Sci., vol. 48, no. 6, pp. 1790-1795, Dec. 2001.
- [38] G. R. Hopkinson, "Proton-induced changes in CTE for n-channel CCDs and the effect on star tracker performance", IEEE Trans. Nucl. Sci., vol. 47, no. 6, pp. 2460-2465, Dec. 2000.